Scaling studies of H-mode pedestal characteristics on Experimental Advanced Superconducting Tokamak

Teng Fei Wang, Qing Zang, Xiao Feng Han, Shu Mei Xiao, Bao Gang Tian, Ai Lan Hu, and Jun Yu Zhao

Citation: Physics of Plasmas **23**, 032509 (2016); doi: 10.1063/1.4944922
View online: http://dx.doi.org/10.1063/1.4944922
View Table of Contents: http://aip.scitation.org/toc/php/23/3
Published by the American Institute of Physics

Scaling studies of H-mode pedestal characteristics on Experimental Advanced Superconducting Tokamak

Teng Fei Wang,[a] Qing Zang,[a] Xiao Feng Han, Shu Mei Xiao, Bao Gang Tian, Ai Lan Hu, and Jun Yu Zhao
Institute of Plasma Physics, Chinese Academy of Sciences, Hefei 230031, China

(Received 1 December 2015; accepted 15 March 2016; published online 29 March 2016)

The characteristics of high-confinement mode (H-mode) pedestal are examined on the Experimental Advanced Superconducting Tokamak. It is found that they are closely dependent on each other between electron pedestal characteristics and global parameters for all types of edge localized mode (ELM). The scaling of pedestal temperature based on thermal conduction and pedestal pressure width is carried out. Based on pedestal pressure gradient and pedestal density, six pedestal pressure width models are applied to predict the pedestal temperature height of type I ELMy H-mode. Compared to experimental results, the normalized poloidal beta model is more consistent than other models. © *2016 AIP Publishing LLC*. [http://dx.doi.org/10.1063/1.4944922]

I. INTRODUCTION

The H-mode discharge of fusion plasma was first observed in the ASDEX tokamak.[1] At the edge of the H-mode plasma, it is discovered a region of steep gradients in the temperature and density profile. This region that causes an obvious reduction in local heat and particle transport at the plasma boundary is called the H-mode transport barrier.[2–5] The height of the transport barrier is called the pedestal.[6–8] The pedestal position is the transition point between the edge of the plasma and the more gentle gradients of the core plasma. In the pedestal local region, the plasma energy confinement is increased, so it is important to investigate the pedestal structure.

In Experimental Advanced Superconducting Tokamak (EAST), the pedestal structure can be measured by the Thomson scattering (TS) system[9–13] that contains data every 20 ms in a typical discharge. This paper mainly studies EAST experimental discharges with plasma current of 300–500 KA. These discharges are low hybrid and neutral beam heated with absorbed power 2–5 MW. The density is in the range of $0.3 < n/n_{GREENWALD} < 0.8$.

For the analysis presented here, it is characterizing the pedestal with a hyperbolic tangent function as described in Sec. II. In Sec. III, there is an obvious correlation between plasma global parameters and pedestal feature. Type I edge localized mode (ELM) pedestal models are given in Sec. IV. Section V presents the result of the analysis, followed by some discussion on physical models. Finally, a summary is drawn in Sec. VI.

II. PEDESTAL ANALYSIS METHOD

The pedestal profiles are characterized by their height, width, and gradient. It is convenient to characterize the pedestal with some functions, and the common function to analyze pedestal structure[14–18] is the hyperbolic tangent function (tanh).[19] This method consists of a hyperbolic tangent function in the pedestal region and a polynomial in the core region. The parameters of the method provide a quantitative way to show the interesting characteristics of pedestal.

At present, EAST TS data contain 13 points in the plasma pedestal region, as shown in Figure 1. The pedestal electron temperature data are fitted with tanh function.

In statistics, root mean-square error (RMSE) represents the difference between the experimental data and the values predicted by the model. In order to quantify the comparison between the prediction scaling value and experimental data, the RMSE is defined as

$$\mathrm{RMSE}(\%) = 100 \times \sqrt{\frac{1}{N-1}\sum_{i=1}^{N}\left(\ln\left(T_{\exp(i)}\right) - \ln\left(T_{\mathrm{mod}(i)}\right)\right)^2}, \tag{2.1}$$

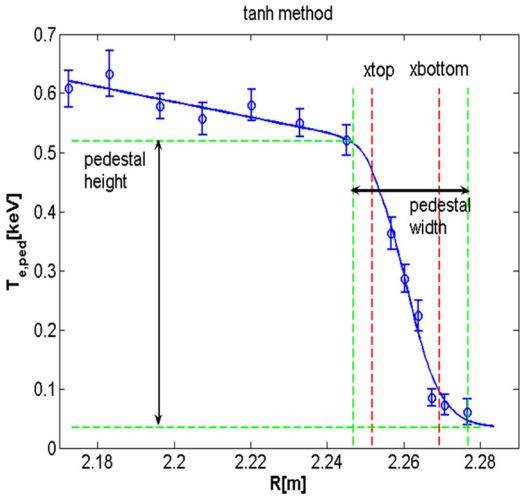

FIG. 1. Definition of fit function based on hyperbolic tangent (tanh) method. Circular points represent EAST Thomson scattering experimental data and error bar. Solid line is fit of tanh function and dashed line is pedestal parameters.

[a]Authors to whom correspondence should be addressed. Electronic addresses: wtf@ipp.ac.cn and zangq@ipp.ac.cn

where N, $T_{\exp}$, and T_{mod} are number of total data points, experimental data, and prediction scaling result, respectively.

III. PEDESTAL SCALING

A. Scaling of pedestal density and temperature with global parameters

The density profile between the edge and the magnetic axis is generally rather flat in H-mode discharges, because the source of gas is from the plasma edge to core. Therefore, it is assumed that the pedestal density is a linear relation with the averaged electron density ($\langle n_e \rangle$). A simple empirical model $n_{e,ped} = k * \langle ne \rangle$ is used in this paper. It is found that the value k = 0.752 is best with a minimum logarithmic RMSE of 16.8%, as shown in Figure 2(a). In Figure 2(b), the deuterium type I ELM is selected and the minimum RMSE is 16.9% with k = 0.786. There is a close relationship between plasma global parameters and pedestal temperature. The H-mode energy confinement factor, named H98, is defined as

$$\mathrm{H98} = \frac{\mathrm{W_{th}}/P_{abs}}{\tau_{th,98y2}}, \tag{3.1}$$

where $\mathrm{W_{th}}$ is the total energy and P_{abs} is the total absorbed power. The IPB98(y,2) scaling for the thermal energy confinement time is given as[20]

$$\tau_{\mathrm{th},98y2} = 0.0562\mathrm{Ip}^{0.93} B_T{}^{0.15} \langle n_e \rangle^{0.41} \times P_{loss}{}^{-0.69} R^{1.97} \varepsilon^{0.58} \kappa^{0.78} M^{0.19}, \tag{3.2}$$

where Ip, $\mathrm{B_T}$, P_{loss}, R, ε, κ, and M are plasma current (MA), toroidal magnetic field (T), heating power (MW), major radius (m), aspect ratio, elongation, and average hydrogenic mass, respectively. As shown in Figure 3(a), the pedestal temperature increases with H98 and plasma current as a result of the increased pedestal energy. In order to reduce the spread in pedestal temperature for the different plasma currents, pedestal density is normalized to the Greenwald density and the pedestal temperature decreases proportionally with the normalized density, as shown in Figure 3(b).

B. Scaling of pedestal temperature based on thermal conduction

The total pedestal energy has been provided by EAST for a large number of observations, whilst only the electron energy ($W_{e,ped}$) is given for the bulk of data. Therefore, it is illustrated in Figure 4(a) that the electron pedestal temperature increases with the pedestal stored energy (W_{ped}) rise based on assuming $W_{ped} = 2W_{e,ped}$ in the pedestal region. The thermal conduction model of pedestal is based on following cases: thermal conduction down the steep temperature gradient is the main energy loss of pedestal comparing to the energy lost of ELM. And so, fitting to all types of H-mode ELM, it was found that the pedestal stored energy is

$$\mathrm{W_{ped}}[\mathrm{MJ}] = 0.0064 * Ip^{1.02} * R^{-0.92} * P^{0.145} \times \langle ne \rangle^{0.35} * Bt^{-0.03} * k^{2.42} * \varepsilon^{-1} * Fq^{1.03}, \tag{3.3}$$

where Fq is the shaping factor (Fq = q95/qcyl, qcyl is the cylindrical safety factor defined as $5\kappa a^2 B/RI$). This scaling satisfies both the Kadomtsev and thermal conduction model of pedestal database DB3V27.[20] Based on previous research, the pedestal temperature is correlated with global parameters, and we cannot find any single-parameter to represent the pedestal temperature. Furthermore, the combination of some global parameters is tried to fit the pedestal temperature, and one pedestal temperature model is as follows:

$$\mathrm{T_{e,ped}}[keV] = W_{ped}/(3\mathrm{k}n_{\mathrm{e,ped}} * 0.92V), \tag{3.4}$$

where k is the Boltzmann constant and V is the plasma volume. The constant of 0.92 is the fraction of the total volume occupied by the pedestal.[21] By combining Eqs. (3.3) and (3.4) with some algebra, the pedestal temperature model can be given. This thermal conduction pedestal temperature model formula yields the RMSE of 24.6% with the EAST data in Figure 4(b).

C. Scaling of pedestal pressure width

The H-mode transport barrier considered the suppression of turbulence in the plasma edge, and the distance from

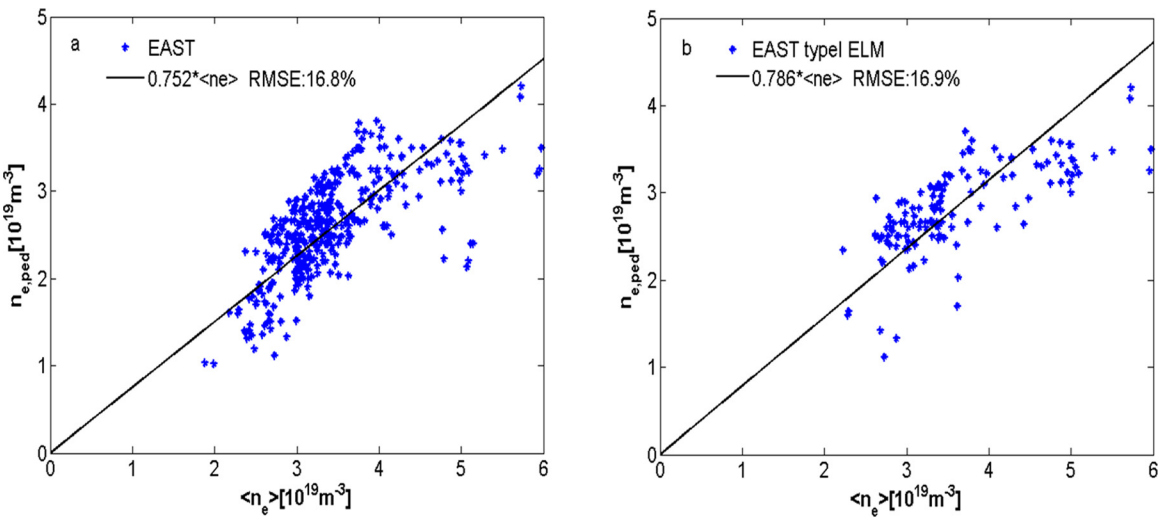

FIG. 2. The pedestal density value compare with the line averaged electron density. (a) All of the H-mode EAST data. (b) Only type I ELM data.

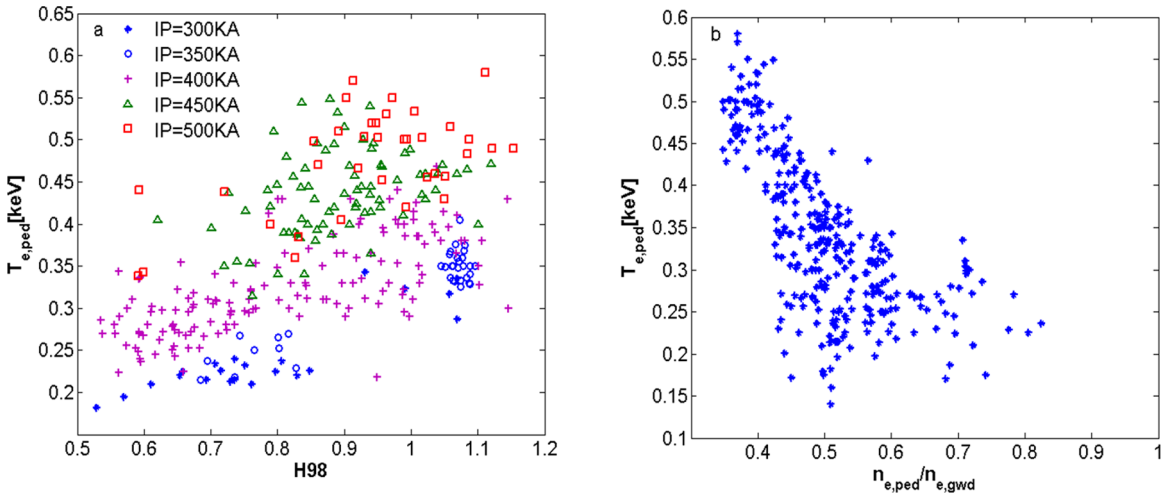

FIG. 3. (a)Variation of pedestal temperature with H98 for different plasma currents. (b) Variation of pedestal temperature with the normalized density.

the innermost suppression point to separatrix is defined to be the width of the H-mode transport barrier. In this part, two dimensionless parameters of the pedestal pressure width are examined and an empirical scaling of the pedestal pressure width as a better fitting of the EAST data is derived. The width scaling relations presented here apply to all types of EAST ELMy H-mode data.

There is some relation between the electron pedestal pressure width and the other edge plasma parameters. The tanh functional form parameters and magnetic equilibrium reconstructions have effect on the pedestal width.[19] The width also has a significant correlation with plasma current and electron pedestal pressure. But the general range of pressure width is 1.5–3.5 cm in EAST, and this small range makes it difficult to find an effective scaling for those parameters.

In order to define the pedestal width, the dimensionless parameters are used. Figure 5 shows pressure width against ion gyro radius (ρ_i) and normalized poloidal beta ($\beta_{p,ped}$),assuming that Te = Ti[22] in the pedestal region and all the ions are deuterium. Figure 6 illustrates the EAST pressure pedestal width scale with dimensionless and configuration parameters in Eq. (3.5). υ_i is the ion collisionality and Fq is the shaping factor. From statistical grounds, the quality of normalized poloidal beta fit is more suitable to describe the pedestal pressure width

$$\Delta_{pe}/R = 0.0233 * \rho_i^{0.31} * \upsilon_i^{-0.012} * \beta_{p,ped}^{-0.018} * fq^{-3.54} * \kappa^3 \times \text{RMSE}: 22.9\%. \quad (3.5)$$

IV. TYPE I ELM MODELS FOR THE PEDESTAL TEMPERATURE

Figure 1 shows the pedestal structure. It is found that the pedestal pressure rise is not only an increase in the pedestal pressure gradient but also an increase in the pedestal width. If the pressure gradient within the pedestal region is constant, then an increase in the pedestal width would automatically mean an increase in the pedestal height.[23] Therefore, the pedestal pressure top is as follows:

$$P_{ped} = 2n_{ped}kT_{ped} = \Delta\left|\frac{\partial p}{\partial r}\right|, \quad (4.1)$$

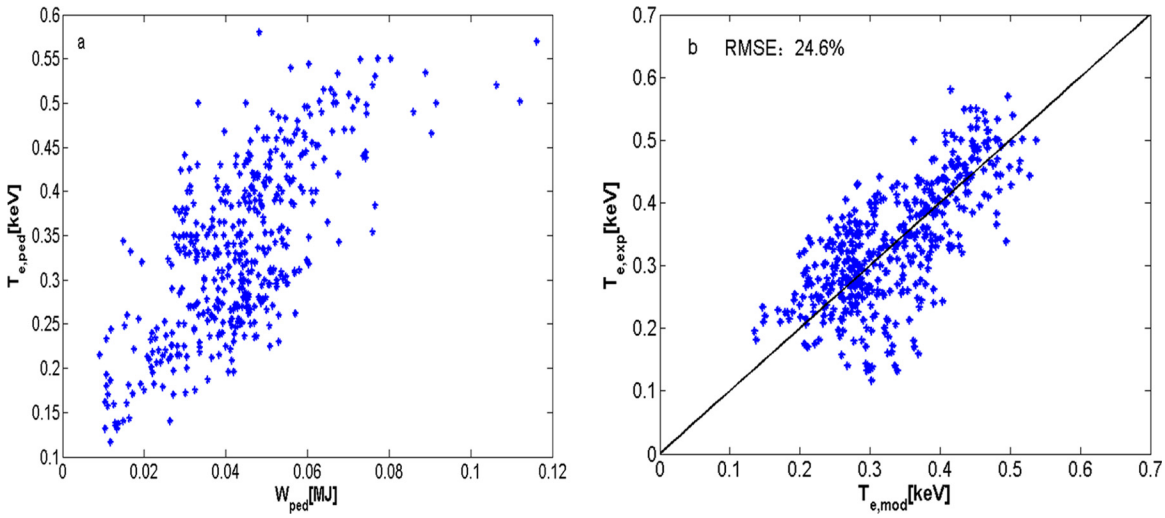

FIG. 4. (a) The pedestal stored energy correlated with electron pedestal temperature. (b) Compare the experimental pedestal temperature with the result of thermal conduction temperature model based on Eqs. (3.3) and (3.4).

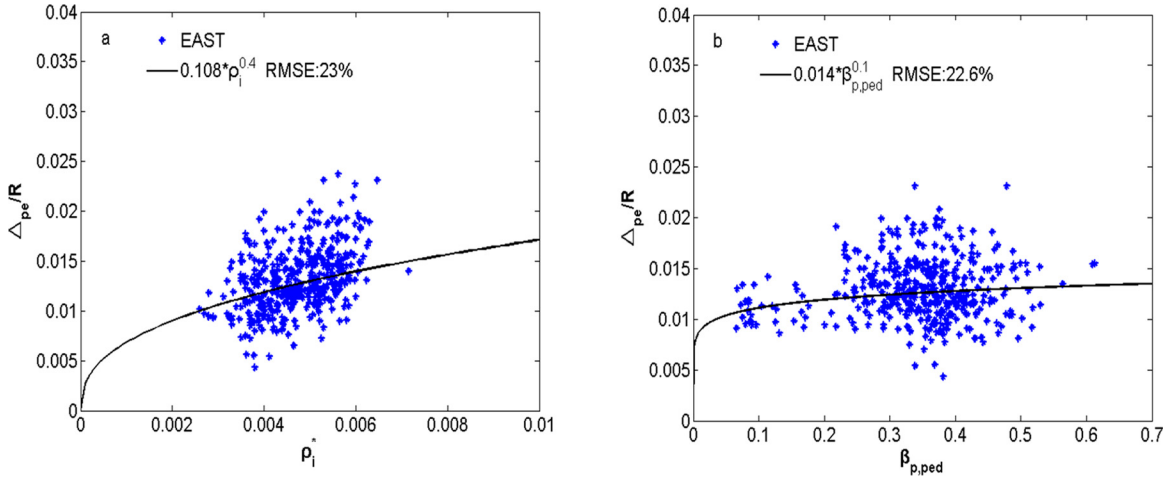

FIG. 5. Pedestal pressure width on the outboard midplane defined by dimensionless parameters. (a) Ion gyro radius, (b) normalized edge poloidal beta. The coefficients are set to a value that has minimum logarithmic root mean square deviation.

where k is the Boltzmann constant, Δ is the pedestal pressure width, and $|\partial p/\partial r|$ is the pressure gradient. Based on pedestal density, pressure width and pressure gradient, the pedestal temperature can be obtained. It is assumed that the pressure gradient is approximately the critical pressure gradient[24] for the first ballooning mode instability (Eq. (4.2)) in EAST type I ELMy H-mode discharges. The safety factor q and the magnetic shear s are calculated in the pedestal width point away from the separatrix. R is the major radius, B_T is the vacuum toroidal magnetic field, κ_{95} is the elongation at the 95% magnetic surface ($\kappa_{95} = 0.914\kappa$), and δ_{95} is the triangularity at the 95% magnetic surface ($\delta_{95} = 0.914\delta$). The safety factor q is given in Eq. (4.3), where $r = a - \Delta$ and the magnetic shear $s_0 = (r/q)\partial q/\partial r$. The magnetic shear in pedestal region contains the effect of normalized collisionality and bootstrap current ($s = s_0(1 - \pi r^2 j_b/I_p)$). The pedestal density is obtained from Figure 2(b). So, the focus of this part is to examine models for estimating the pedestal pressure width.

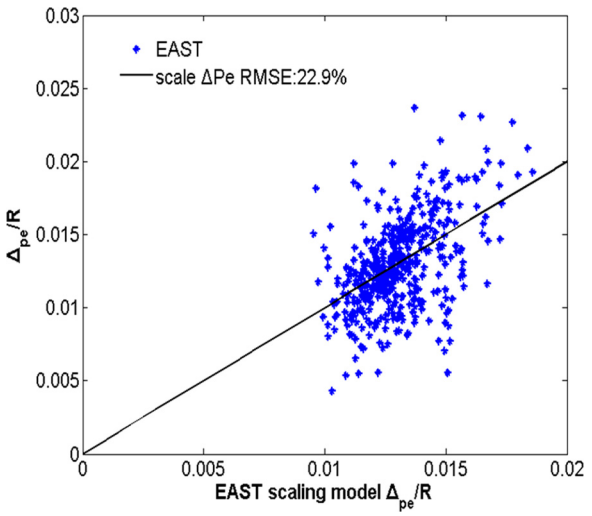

FIG. 6. The electron pedestal pressure width scale with dimensionless and configuration parameters in Eq. (3.5).

$$\left(\frac{\partial p}{\partial r}\right) = \left(\frac{\partial p}{\partial r}\right)_c = -\left(B_T^2/2\mu_0 R q^2\right) * \left(0.4s\left(1 + \kappa_{95}^2\left(1 + 5\delta_{95}^2\right)\right)\right), \tag{4.2}$$

$$q(r) = \left(\frac{0.85a^2 B_T}{IR}\right) \times \left(\frac{1 + \kappa_{95}^2\left(1 + 2\delta_{95}^2 - 1.2\delta_{95}^3\right)(1.17 - 0.65a/R)}{\left[1 - (a/R)^2\right]^2}\right) \times \left\{\left[1 + \left(\frac{r}{1.4R}\right)^2\right]^2 + 0.27\left|\ln\left(\frac{1-r}{a}\right)\right|\right\}. \tag{4.3}$$

Based on the pedestal pressure gradient and pedestal density, six pedestal pressure width models are applied to predict the pedestal temperature height of type I ELMy H-mode. In Section III, dimensionless parameters with pedestal pressure width are measured. Therefore, model 1[25] is based on the assumption that the magnetic well stabilizes edge turbulence, and Osborne proposed the scaling of form

$$\Delta \propto c1 * \sqrt{\beta_p} * R, \tag{4.4}$$

where β_p is the normalized edge poloidal beta, while constant c1 is chosen so as to optimize the agreement between the measured values of $T_{e,ped}$ and the model results for $T_{e,ped}$ by minimizing the RMSE. By combining Eqs. (4.1)–(4.4) with some algebra, the pedestal temperature can be obtained as follows:

$$T_{e,ped} = c1^2 * (1.244 \times 10^{21}) * \left(\frac{B}{q(x)}\right)^4 \left(\frac{a\pi(1+\kappa)}{\mu_0 I p}\right)^2 \left(\frac{\alpha_c(x)^2}{n_{ped}}\right), \tag{4.5}$$

where x is the position of the pedestal temperature value. Figure 7 illustrates the comparison between the pedestal temperature from the width model 1 and experimental data.

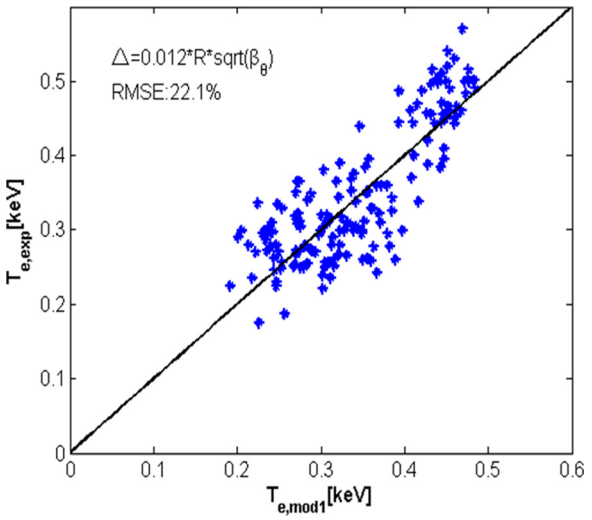

FIG. 7. The pedestal temperature predicted by poloidal pressure model compared with experimental type I ELM data.

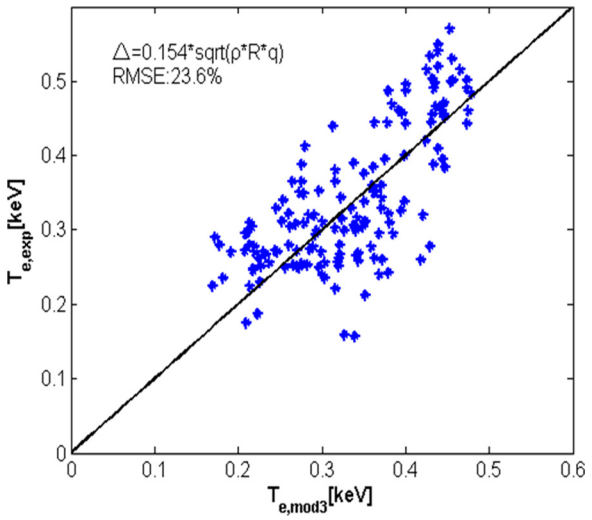

FIG. 9. The pedestal temperature predicted by flow shear stabilization model compared with experimental type I ELM EAST data.

Model 2 is based on magnetic and flow shear stabilization.[26] It is assumed that the turbulence is suppressed when the E × B shearing rate is equal to the maximum linear growth rate at the top of the H-mode pedestal. The pedestal width scales as

$$\gamma_{\mathrm{Er\times B}} \approx \frac{\rho c_s}{\Delta^2} = \frac{c_s}{\Delta}\frac{1}{s^2} \approx \gamma_{\max} \qquad \Delta \propto c2 * \rho * s^2, \tag{4.6}$$

where ρ is the gyro radius and s is the magnetic shear. Compared with experimental data, the pedestal temperature from the width model 2 is shown in Figure 8. The model 3 is based on flow shear stabilization.[23] This model is similar to model 2, while Er × B suppression of long wavelength modes is assumed to be the relevant factor in establishing the edge transport barrier. Therefore, the pedestal width scales as

$$\gamma_{\mathrm{Er\times B}} \approx \frac{\rho c_s}{\Delta^2} = \frac{c_s}{qR} \approx \gamma_{local} \qquad \Delta \propto c3 * \sqrt{\rho R q}, \tag{4.7}$$

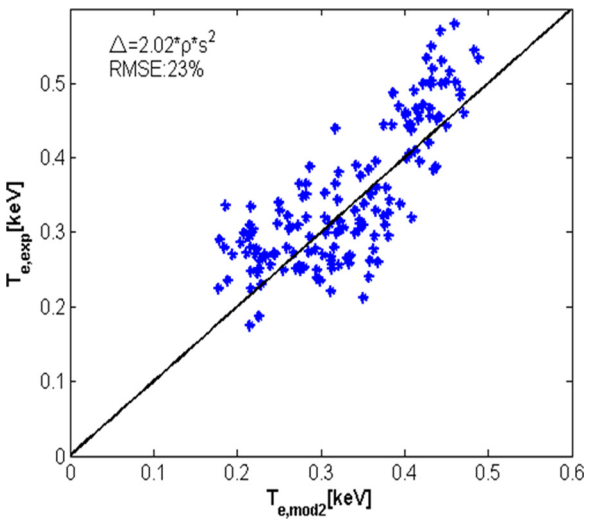

FIG. 8. The pedestal temperature predicted by magnetic and flow shear stabilization model compared with experimental type I ELM EAST data.

where R is the major radius and q is the safety factor in the pedestal position. The pedestal temperature from the width model 3 is shown in Figure 9. Model 4 is based on the diamagnetic stabilization model.[27] Model 5 is based on the neutral penetration.[24] The neutrals can penetrate inside the separatrix to affect the H-mode pedestal region. In this model, the pedestal width is defined as the length of neutral particles penetrating into the plasma. Therefore, the pedestal width is inversely proportional to the pedestal density value. Model 6 is Shaing's model[28] based on ion orbit loss, the predicted pressure width of the pedestal is proportional to aspect ratio and ion poloidal gyro radius. The comparison between the six pedestal temperature models and experimental data is illustrated in Table I. The normalized poloidal pressure model 1 yields the lowest RMSE for EAST experimental data.

V. RESULTS AND DISCUSSION

The RMSE in Table I ranges from 22% to 31%. The model is based on the normalized edge poloidal pressure that yields the lowest RMSE and the ion orbit loss model that yields the highest RMSE. It is difficult to find obvious differences among the normalized edge poloidal pressure model, magnetic/flow shear stabilization model, and flow shear stabilization model. Therefore, further approach is carried out to make a distinction.

The theory analysis indicates that the normalized edge poloidal beta, gyro radius, pedestal density, and related quantities are correlated with the pedestal pressure width.

Based on neutral penetration, the pedestal width is inversely proportional to the pedestal density value in model 5. However, the distribution of the density is much broader than other parameters, and the gas puff can cause an increase in the pedestal density. Therefore, the neutral penetration width model does not suit to EAST. Model 1 is based on the normalized edge poloidal beta, while models 2 and 3 are relative to gyro radius. The normalized edge poloidal beta and gyro radius are defined as

TABLE I. Six theory models for the pedestal width are applied in determining the pedestal temperatures that are compared with EAST experimental data.

Width scaling	Pedestal temperature RMSE	Physic basis
$\Delta = 0.012 * \sqrt{\beta_p} * R$	22.1%	Normalized poloidal pressure
$\Delta = 2.02 * \rho s^2$	23%	Magnetic and flow shear stabilization
$\Delta = 0.154 * \sqrt{\rho R q}$	23.6%	Flow shear stabilization
$\Delta = 1.115 * \rho^{2/3} R^{1/3}$	29%	Diamagnetic stabilization
$\Delta = 0.044/n_{ped}$	28.2%	Neutral penetration
$\Delta = 1.734 * \sqrt{\varepsilon} * \rho_\theta$	31%	Ion orbit loss

$$\beta_{e,ped} \propto P_{e,ped}/\langle B_p \rangle^2$$
$$\rho \propto Ti/(aB_{t,ped}), \quad (5.1)$$

where $\langle B_p \rangle = \mu_0 Ip/l_{lcfs}$ is the flux surface averaged poloidal field, with l_{lcfs} as the length of the last closed flux surface, $B_{t,ped} = B_{t0}/(1+\varepsilon)$. It is found that the essence of the normalized edge poloidal beta and gyro radius is the pedestal pressure ($P_{e,ped}$) and pedestal temperature ($T_{e,ped}$), respectively. The pedestal density ($n_{e,ped}$) is varied but other parameters are kept similar to determine whether a scaling of pedestal pressure width (Δ_{pe}) with $P_{e,ped}$ or $T_{e,ped}$ is more suitable. Figure 10 shows that Δ_{pe} and $P_{e,ped}$ increase with the $n_{e,ped}$, while $T_{e,ped}$ slightly drop. From this results, we conclude that $P_{e,ped}$ is likely to be consistent with Δ_{pe}. In a word, model 1 based on the normalized edge poloidal beta is more suitable for EAST than other models.

Plasma shape such as triangularity and elongation could influence plasma pedestal evidently. A related question is whether there are any significant differences between H-mode discharges with a single-null divertor and a double-null divertor. Model 1 is a semi-empirical scaling based on the normalized edge poloidal beta. The pressure at the top of the H-mode pedestal increases strongly with triangularity, primarily due to an increase in the margin by which the edge pressure gradient exceeds the ideal ballooning mode first stability limit.[16] Therefore, an effective way to verify this model is to scan a large range of elongation and triangularity because the normalized edge poloidal beta is varied with the shape of the plasma. At present, the range of EAST configuration parameter is narrow, and it is very useful to expand the range of these parameters in the EAST pedestal database.

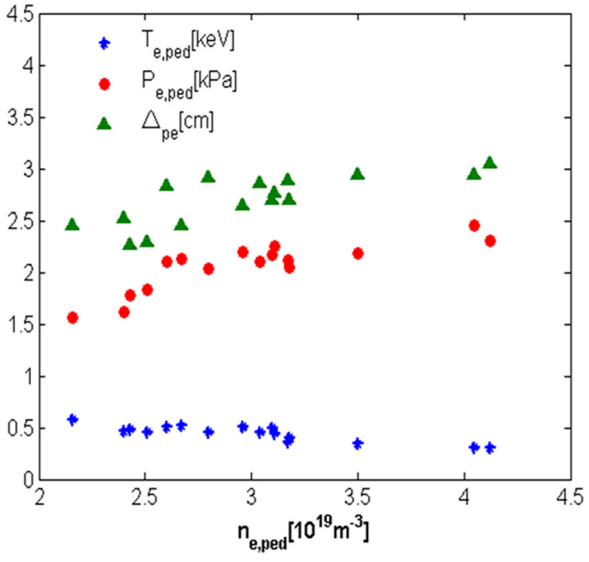

FIG. 10. The varied of pedestal density plot against the electron temperature, pressure at the top of the H-mode pedestal, and the electron pressure. These discharges are similar to plasma current 500 KA, the toroidal field 2.5 T, and low hybrid and neutral beam heated with absorbed power 3.9–4.1 MW.

Isotope scans can help to test model 2 and model 3 because it could vary the ion gyro radius, and previous studies have stated clearly the dependence of the pedestal height on isotopes. It would be very useful if a large data of hydrogen and deuterium discharges are provided.

VI. SUMMARY AND CONCLUSION

The H-mode pedestal characteristics on EAST are measured in a range of plasma conditions using Thomson scattering system. This paper has described the results of the H-mode pedestal in the EAST tokamak. The hyperbolic tangent function is applied to analyze pedestal characteristics. For EAST H-mode discharges, the electron pedestal height is correlated with plasma global parameters. It is difficult to find any single-parameter for describing the characterization of the pedestal temperature height so that the combination of some global parameters can better describe the pedestal height. The height of the electron pedestal temperature is proportional to the pedestal stored energy and the latter can be scaled with global parameters. Therefore, the scaling of pedestal temperature based on thermal conduction is carried out. The general range of pedestal pressure width is 1.5–3.5 cm in EAST, and this small range makes it difficult to find an effective scaling for plasma global parameters. So, dimensionless parameters of the plasma, especially normalized poloidal beta, are used to describe pedestal pressure width.

On EAST type I ELMy H-mode, models that predict the pedestal temperature height are applied. Those models needed pedestal pressure width, gradient, and pedestal density. The pedestal pressure gradient is assumed to be approximately for the first ballooning mode instability and the pedestal density is from EAST experimental data. The six models of pedestal pressure width are given to calculate the pedestal temperature height. The normalized poloidal beta model consistent with experimental results is better than

other models. It should be effective to verify pedestal temperature model based on plasma shape and isotope. It will be very important to expand the parameters range of EAST pedestal database in the future.

ACKNOWLEDGMENTS

This work was funded by the National Natural Science Foundation of China with Contract Nos. 11275233 and 11405206, National Magnetic Confinement Fusion Science Program of China under Grant Nos. 2013GB112003, and Science Foundation of Institute of Plasma Physics, Chinese Academy of Sciences, China, under Grant No. DSJJ-15-JC01.

[1]F. Wagner, G. Becker, K. Behringer, D. Campbell, A. Eberhagen, W. Engelhardt, G. Fussmann, O. Gehre, J. Gernhardt, G. V. Gierke, G. Haas, M. Huang, F. Karger, M. Keilhacker, M. Kornherr, K. Lackner, G. Lisitano, G. G. Lister, H. M. Mayer, and D. Meisel, Phys. Rev. Lett. **49**, 1408 (1982).
[2]P. Gohil, L. R. Baylor, K. H. Burrell, T. A. Casper, E. J. Doyle, C. M. Greenfield, T. C. Jernigan, J. E. Kinsey, C. J. Lasnier, R. A. Moyer, M. Murakami, T. L. Rhodes, D. L. Rudakov, G. M. Staebler, G. Wang, J. G. Watkins, W. P. West, and L. Zeng, Plasma Phys. Controlled Fusion **45**, 601–620 (2003).
[3]K. C. Shaing, E. C. Crume, Jr., and W. A. Houlberg, Phys. Fluids B **2**, 1492 (1990).
[4]R. E. Waltz, G. D. Kerbel, J. Milovich, and G. W. Hammett, Phys. Plasmas **2**, 2408 (1995).
[5]X. H. Wang, P. H. Diamond, and M. N. Rosenbluth, Phys. Fluids B **4**, 2402 (1992).
[6]H. Urano, Nucl. Fusion **54**, 116001 (2014).
[7]W. M. Stacey and R. J. Groebner, Phys. Plasmas **13**, 012513 (2006).
[8]H. Urano, N. Oyama, K. Kamiya, Y. Koide, H. Takenaga, T. Takizuka, M. Yoshida, Y. Kamada, and JT-60 Team, Nucl. Fusion **47**, 706 (2007).
[9]Q. Zang, J. Y. Zhao, L. Yang, Q. S. Hu, Y. Q. Jia, T. Zhang, X. Q. Xi, S. H. BHATTI, and X. Gao, Plasma Sci. Technol. **12**, 144 (2010).
[10]H. Chen, J. Y. Zhao, Q. Zang, S. M. Xiao, A. L. Hu, X. F. Han, and T. F. Wang, J. Fus. Energy **34**, 9 (2015).
[11]X. F. Han, C. Q. Shao, X. Q. Xi, J. Y. Zhao, Q. Zang, J. H. Yang, X. X. Dai, and S. Kado, Rev. Sci. Instrum. **84**, 053502 (2013).
[12]C. Q. Shao, J. Y. Zhao, Q. Zang, H. F. Han, X. Q. Xi, J. H. Yang, H. Chen, and A. L. Hu, Plasma Sci. Technol. **16**, 721 (2014).
[13]Q. Zang, C. L. Hsieh, J. Y. Zhao, H. Chen, and F. J. Li, Rev. Sci. Instrum. **84**, 093504 (2013).
[14]R. J. Groebner and T. H. Osborne, Phys. Plasmas **5**, 1800 (1998).
[15]Y. Kamada, H. Takenaga, A. Isayama, T. Hatae, H. Urano, and H. Kubo, Plasma Phys. Controlled Fusion **44**, A279 (2002).
[16]T. H. Osborne, J. R. Ferron, R. J. Groebner, L. L. Lao, A. W. Leonard, M. A. Mahdavi, R. Maingi, R. L. Miller, A. D. Turnbull, M. Wade, and J. Watkins, Plasma Phys. Controlled Fusion **42**, A175 (2000).
[17]W. M. Stacey, Phys. Plasmas **11**, 4295 (2004).
[18]A. W. Leonard, R. J. Groebner, T. H. Osborne, and P. B. Snyder, Phys. Plasmas **15**, 056114 (2008).
[19]P. A. Schneider, E. Wolfrum, R. J. Groebner, T. H. Osborne, M. N. A. Beurskens, M. G. Dunne, J. R. Ferron, S. Günter, B. Kurzan, K. Lackner, P. B. Snyder, H. Zohm, ASDEX Upgrade Team, DIII-D Team, and JET EFDA Contributors, Plasma Phys. Controlled Fusion **54**, 105009 (2012).
[20]ITER Physics Expert Groups on Confinement and Transport and Confinement Modelling and Database, Nucl. Fusion **39**, 2175 (1999).
[21]K. Thomsen, J. G. Cordey, H-mode Database Working Group, and Pedestal Database Working Group, Plasma Phys. Controlled Fusion **44**, A429 (2002).
[22]G. Q. Li, Q. L. Ren, J. P. Qian, L. L. Lao, S. Y. Ding, Y. J. Chen, Z. X. Liu, B. Lu, and Q. Zang, Plasma Phys. Controlled Fusion **55**, 125008 (2013).
[23]M. Sugihara, V. Mukhovatov, A. Polevoi, and M. Shimada, Plasma Phys. Controlled Fusion **45**, L55 (2003).
[24]T. Onjun, G. Bateman, A. H. Kritz, and G. Hammett, Phys. Plasmas **9**, 5018 (2002).
[25]T. H. Osborne, K. H. Burrell, R. J. Groebner, L. L. Lao, A. W. Leonard, R. Maingi, R. L. Miller, G. D. Porter, G. M. Staebler, and A. D. Turnbull, J. Nucl. Mater. **266–269**, 131 (1999).
[26]M. Sugihara, Y. Igitkhanova, G. Janeschitza, A. E. Hubbardb, Y. Kamadac, J. Lingertatd, T. H. Osbornee, and W. Suttropf, Nucl. Fusion **40**, 1743 (2000).
[27]B. N. Rogers and J. F. Drake, Phys. Plasmas **6**, 2797 (1999).
[28]K. C. Shaing, Phys. Fluids B **4**, 290 (1992).